Structure and reactivity of a siderophore-interacting protein from the marine bacterium *Shewanella* reveals unanticipated functional versatility

Received for publication, August 1, 2018, and in revised form, November 5, 2018 Published, Papers in Press, November 12, 2018, DOI 10.1074/jbc.RA118.005041

Inês B. Trindade[‡], José M. Silva[‡], Bruno M. Fonseca[‡], Teresa Catarino[‡§], Masaki Fujita[¶], Pedro M. Matias[‡‖], Elin Moe[‡], and Ricardo O. Louro[‡1]

From the [‡]Instituto de Tecnologia Química e Biológica António Xavier (ITQB-NOVA), Universidade Nova de Lisboa, Av. da República (EAN), 2780-157 Oeiras, Portugal, the [§]Departamento de Química, Faculdade de Ciências e Tecnologia, Universidade Nova de Lisboa, 2829-516, Caparica, Portugal, the [¶]Faculty of Fisheries Sciences, Hokkaido University, 3-1-1 Minato-cho, Hakodate, Hokkaido 041-8611, Japan, and the [‖]Instituto de Biologia Experimental e Tecnológica (iBET), Apartado 12, 2780-901 Oeiras, Portugal

Edited by Chris Whitfield

Siderophores make iron accessible under iron-limited conditions and play a crucial role in the survival of microorganisms. Because of their remarkable metal-scavenging properties and ease in crossing cellular envelopes, siderophores hold great potential in biotechnological applications, raising the need for a deeper knowledge of the molecular mechanisms underpinning the siderophore pathway. Here, we report the structural and functional characterization of a siderophore-interacting protein from the marine bacterium *Shewanella frigidimarina* NCIBM400 (SfSIP). SfSIP is a flavin-containing ferric-siderophore reductase with FAD- and NAD(P)H-binding domains that have high homology with other characterized SIPs. However, we found here that it mechanistically departs from what has been described for this family of proteins. Unlike other FAD-containing SIPs, SfSIP did not discriminate between NADH and NADPH. Furthermore, SfSIP required the presence of the Fe^{2+}-scavenger, ferrozine, to use NAD(P)H to drive the reduction of *Shewanella*-produced hydroxamate ferric-siderophores. Additionally, this is the first SIP reported that also uses a ferredoxin as electron donor, and in contrast to NAD(P)H, its utilization did not require the mediation of ferrozine, and electron transfer occurred at fast rates. Finally, FAD oxidation was thermodynamically coupled to deprotonation at physiological pH values, enhancing the solubility of ferrous iron. On the basis of these results and the location of the SfSIP gene downstream of a sequence for putative binding of aerobic respiration control protein A (ArcA), we propose that SfSIP contributes an additional layer of regulation that maintains cellular iron homeostasis according to environmental cues of oxygen availability and cellular iron demand.

This work was supported by the European Union's Horizon 2020 research and innovation program under Grant 810856, National Funds Grant ERA-MBT/0003/2014, Ph.D. fellowship PD/BD/135187/2017 (to I. B. T.), and postdoctoral fellowships SFRH/BPD/94050/2013 and SFRH/BPD/93164/2013 (to E. M. and B. F. M.), through the FCT-Fundação para a Ciência e a Tecnologia. The authors declare that they have no conflicts of interest with the contents of this article.

This article contains Table S1 and Figs. S1–S7.

The atomic coordinates and structure factors (code 6GEH) have been deposited in the Protein Data Bank (http://wwpdb.org/).

[1] To whom correspondence should be addressed: ITQB-NOVA, Av da República (EAN), 2780–157 Oeiras, Portugal. Tel.: 351- 214469332; E-mail: louro@itqb.unl.pt.

The metabolic versatility of the *Shewanella* genus enables these bacteria to thrive in a wide variety of iron-limited environments ranging from the ocean floor all the way to the infection of human hosts (1, 2). *Shewanella* are well-known spoilers of food products, notorious fish pathogens, and *Shewanella oneidensis* has been extensively studied for its remarkable ability of performing extracellular electron transfer (1, 2). Overall, this environmental versatility of *Shewanella* is highly dependent on the ability of these organisms to produce an abundance of iron-rich proteins, mainly multiheme *c*-type cytochromes (3). *Shewanella frigidimarina*, is a psychrophilic bacterial species isolated from Antarctic costal marine environments, in particular, from biofilms (4, 5). The multiheme *c*-type cytochromes of *S. frigidimarina* have been extensively characterized. However, being a marine microorganism, access to iron poses a permanent challenge (6–8).

Iron demand together with scarcity in the ocean limits microbial life, and all the respective biogeochemical processes essential for ocean productivity (9, 10). This high need for iron requires robust strategies for iron uptake while avoiding an uncontrolled oversupply that would be dangerous to organisms that live in oxic–anoxic transition zones (11). However, very limited knowledge exists regarding the iron-uptake strategies used by *Shewanella* in general, and by *S. frigidimarina* in particular. Over a decade ago, various *Shewanella* strains were identified as capable producers of soluble or surface-associated metal chelating compounds designated as siderophores (from the Greek "iron carrier"). This is a strategy of iron uptake that is widespread across the tree of life, but poorly explored in the *Shewanella* genus (12, 13).

Siderophores are low molecular weight compounds with high affinity for ferric-iron (13). These compounds play an essential role in the growth and virulence of many microorganisms. Since their discovery, over 500 distinct siderophores have been identified (14). This diversity reflects a veritable "arms race" to efficiently capture iron from the environment. Indeed, the combination of siderophores produced by an organism is crucial for bacterial competition as well as for the outcome of pathogenesis (15). The siderophore pathway involves the production and export of apo-siderophores (no iron), and their

reuptake as ferric-siderophores (iron-loaded) so that iron is released for utilization in the cell metabolism (13). Within the siderophore pathway, the molecular mechanisms for iron release from the ferric-siderophore complexes remain poorly characterized, but ferric-siderophore reduction appears to be the more widespread mechanism.

In bacteria, ferric-siderophore reduction can occur in the cytosol and involves the superfamily of siderophore-interacting proteins composed of two distinct families: the ferric-siderophore reductase (FSRs)[2] family, and the siderophore-interacting protein (SIPs) family (16, 17). SIPs can be distinguished in two broad groups: one that generates cytosolic reduced free flavins that subsequently reduce the ferric-siderophores, and a second group of SIPs that contain stably attached flavins and use NADH and/or NADPH as reducing agents. The latter includes the first reported SIP, the ViuB from *Vibrio cholerae*, and also other examples such as *Escherichia coli* YqjH and FscN from the Gram-positive bacterium *Thermobifida fusca* (16–20). Additionally, this group of SIPs can be further divided into two subgroups: subgroup I, which utilize NADH as electron donor and subgroup II, which utilize NADPH (16). This division is based upon the differences found in the C-terminal and N-terminal sequences: subgroup I proteins (*e.g.* ViuB, FscN) contain prominent C-terminal α-helix elements, whereas subgroup II contain N-terminal sequence extensions and insertions (*e.g.* YqhJ) (16, 17).

The SIP superfamily, which includes both SIPs and FSRs is widespread across several bacterial genera, however, very few of these proteins have been thoroughly characterized (YqhJ from *E. coli*, FscN from *T. fusca*, and Iruo from *Staphylococcus aureus*) and thus, the specific intracellular fate of the iron-loaded siderophores is among the least understood steps of the siderophore pathway at the molecular level (16, 17, 21). Across the different genomes in the *Shewanella* genus, some species contain genes that code for SIPs only (*e.g. S. frigidimarina* and *Shewanella morhuae*), others code for FSRs only (*e.g. Shewanella oneidensis* and *Shewanella algae*), whereas a few species contain genes that code for both SIPs and FSRs (*e.g. Shewanella putrefaciens* and *Shewanella baltica*). However, no knowledge exists on how these proteins are utilized, their importance and role for iron uptake and regulation. Based on sequence similarity with ViuB from *V. cholerae,* and with the structurally characterized *S. putrefaciens* homologue (SpSIP PBD code 2GPJ), a SIP was identified in *S. frigidimarina* NCIM400 (SfSIP) (22, 23). This work reports its characterization.

[2] The abbreviations used are: FSRs, ferric siderophore reductase family; SfSIP, siderophore-interacting protein from *S. frigidimarina*; SIP, siderophore-interacting protein; ArcA, aerobic respiration control protein A; ViuB, vibriobactin utilization protein; YqjH, siderophore-interacting protein from *E. coli;* FscN, siderophore-interacting protein from the fuscachelin siderophore gene cluster; PDB, Protein Data Bank; BIS, ferric-bisucaberin; AVA, ferric-avaroferrin; PUT, ferric-putrebactin; FER, ferric-ferrioxamine E; LB, Luria-Bertani medium; SHE, standard hydrogen electrode; FchR, ferric citrate and hydroxamate reductase; PFV, protein film voltammetry; DLS, Diamond Light Source; PGE, pyrolytic graphite edge; CHES, 2-(cyclohexylamino)ethanesulfonic acid.

Results

SfSIP belongs to the ViuB subgroup: The proposed NADH-utilizing proteins

The SFRI_RS12295 gene from *S. frigidimarina NCIM400* was inserted into the pETBlue-1 vector (Novagen) and SfSIP was overexpressed and purified by ion-exchange chromatography, as described elsewhere (23). The SDS-PAGE analysis revealed that the purified yellow protein migrated as a single band at 30 kDa, as expected from theoretical calculations based on amino acid and co-factor composition. N-terminal sequence analysis of the purified protein confirmed the identity of SfSIP and the UV-visible spectrum presented the typical features of an oxidized flavoprotein with absorption peaks at 387 and 470 nm (23).

The two subgroups of SIPs can be distinguished based on the length of their C terminus (16, 17). Subgroup I SIPs includes ViuB and FscN from *T. fusca*, and Subgroup II SIPs includes YqjH from *E. coli*. Comparative sequence analysis of SfSIP with its homologues (Fig. S1), revealed that the SfSIP contains a "long" C terminus with prominent α-helix elements. For this reason, it is possible to assign SfSIP to Subgroup I SIPs, which utilize NADH as an electron donor to reduce ferric-siderophores (16, 17). These results were further investigated by analyzing the three-dimensional structure of SfSIP.

Structural characterization of SfSIP

The crystal structure of SfSIP was determined to 1.15 Å resolution and deposited in PDB with accession number 6GEH. The structure reveals two domains, the FAD- and NAD(P)H-binding domains (Fig. 1*A*), as observed for previously determined structures of SIPs from *S. putrefaciens* (PDB code 2GPJ) and *T. fusca* (PDB code 4YHB), which share 32 and 28% sequence identity with SfSIP, respectively (17). The electron density is well-defined from residues Ser-9 to Leu-264, except for residues Pro-120 to Met-123, which are facing the solvent and are in the loop that connects the FAD- and NAD(P)H-binding domains, between strands β6 and β7 (Fig. 1*A*). The FAD-binding domain is composed of five antiparallel β-strands (β7–β11) with two short α-helices (α2 and η3) connecting the long loops. The FAD shows a planar conformation, and thus is oxidized as expected from the color and the spectrum of the sample used for crystallization. The FAD cofactor is well-conserved compared with both structures of YqhJ and FscN and this is stabilized through aromatic stacking interactions of the isoalloxazine ring by Tyr-47, Tyr-75, and Tyr-245 and hydrogen bonds with residues Asp-90 (backbone O), Val-92 (backbone N), and Thr-76 (backbone N). The negatively charged phosphate groups from FAD are also stabilized through hydrogen bonds with Arg-73 (NH_2 and NE), His-96 (side chain NE2), Ala-100 (backbone N), Thr-101 (backbone N), and Ala-252 (N backbone). In addition, the ribose ring forms hydrogen bonds with the backbone of the protein, namely with Thr-250 (N and O backbone), Asn-247 (N backbone), and Lys-247 (O backbone), and with two water molecules (Fig. S2) (24). The NAD(P)H-binding domain consists of six antiparallel β-strands (β1–β6) and two short α-helices (α1 and η1). This has a β1–α1–β2 architecture consistent with the Ross-

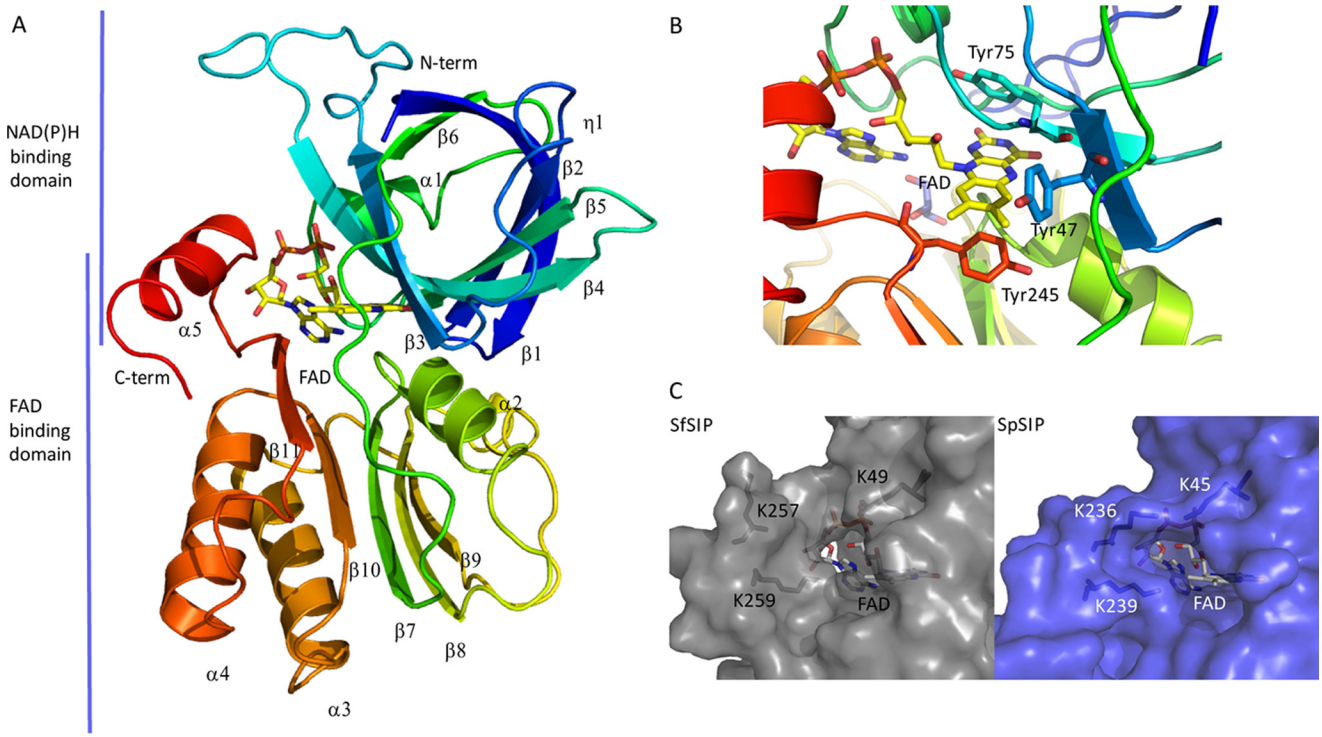

Figure 1. Structural characterization of SIP. *A,* overall structure of SIP; *B,* close-up of the FAD pocket and stacking residues (Tyr-47, Tyr-75, and Tyr-245); *C,* putative NAD(P)H-binding pocket: comparison of the C-terminal helix of SIPs from *S. frigidimarina* (*SfSIP*) and *S. putrefaciens* (*SpSIP*). Lys-236 from SpSIP seems to make a bridge across the pocket, whereas Lys-257 in SfSIP is more distant from the isoalloxazine ring and pointing outwards from the pocket making more space available for substrate binding (ferric-siderophore and/or electron donors).

mann-fold. The C-terminal of SfSIP contains an α-helix as predicted, confirming that SfSIP belongs to the subgroup I of SIPs. Furthermore, it has been proposed that a triad of basic amino acid residues (Lys-45, Lys-236, and Lys-239 based in the primary sequence of *S. putrefaciens*) forms a ferric-siderophore–binding pocket. In SfSIP, both comparative sequence analysis (Fig. S1) and structural determination of SfSIP revealed that it possesses a lysine residue in position 49, and two lysine residues in positions 257 and 259 (Fig. 1*C*). These could serve a similar role as predicted for the potential ferric-siderophore–binding pocket formed by this triad of basic amino acid residues (16). However, Lys-257 is placed in a different position compared with the corresponding lysine in SpSIP (Lys-236), further away from the FAD ring. This further opening of the pocket together with the absence of other surface locations that provide access to the FAD cofactor suggest that this pocket is also the location of NAD(P)H binding. So far no crystal structure has been reported for SIPs in complex with ferric-siderophores or NAD(P)H. In this work the same situation occurred, even though the crystallization was performed in the presence of both molecules. Therefore, the binding site of these substrates in SfSIP remains open to speculation.

SfSIP performs proton-coupled electron transfer

Proteins with a FAD as redox center can couple one- and two-electron transfer reactions with proton transfer. In SfSIP, this ability was investigated using protein film voltammetry (PFV), resulting in well-defined voltammetric responses (Fig. S3*A*). The width at half-height and midpoint potentials of the voltammetric signals are reported in Table 1 (25).

Table 1
Redox properties of SfSIP at various pH values

pH	Width at half-height peak	$E(0)$
	mV	
5.4	86 ± 6	−130
6.3	96 ± 1	−201
7.0	94 ± 6	−228
7.8	102 ± 6	−286
8.5	110 ± 3	−320

The data reveal that SfSIP presents a redox–Bohr effect (Fig. S3*B* and Table 1). The simulation of pH dependence of the reduction potentials (Fig. S3*B*) shows that the pK_a values must be lower than 4.5 for pK_{aox} and higher than 10 for pK_{ared}, outside of the pH range that could be tested (26). These results mean that in the physiological range of *S. frigidimarina* the release of electrons by SfSIP is accompanied by the release of protons. Because both electrons and protons originate from the isoalloxazine ring, this coupling provides a localized pH drop that enhances iron solubility. The reduction potential of SfSIP changes by 57 ± 2 mV for every pH unit and the half-height width of the anodic and cathodic signals was close to the theoretical value of 90 mV (Table 1) predicted for a Nernstian equilibrium for a proton coupled-one electron transfer (3.53 *RT*/nF). Trumpet plots were fitted (Fig. S4) using the Butler-Volmer model for 1 electron transfer, and proton transfer is not the limiting process at any pH value tested (27, 28). Furthermore, at pH 7 the reduction of SfSIP by NADH and NADPH (−320 mV *versus* SHE) should be feasible, however, both of these nucleotides perform a 2-electron step reduction, and this was not observed in PFV measurements.

Table 2
Midpoint reduction potentials of ferric-siderophores used in this study

Siderophore	pH, temperature	$E_{1/2}$ (mV *vs* SHE)	Reference
Avaroferrin	7.25, 25 °C	−295 and +25	This study
Bisucaberin	7.30, 25 °C	−311 and +35	This study
Ferrioxamine E	10.5, ND[a]	−478	30
Putrebactin	7.27, 25 °C	−309 and +33	This study

[a] ND, not determined.

SfSIP, a ferric siderophore reductase

To test SfSIP as a ferric siderophore reductase, siderophores, the putative substrates of SfSIP were produced and characterized (29). Three siderophores produced by *Shewanella* were obtained: a 4.3 mg of pure sample of bisucaberin, a 5.2 mg sample of of avaroferrin containing small traces of bisucaberin, and a sample of putrebactin containing small traces of the previous two siderophores. The addition of iron to the apo-siderophores resulted in an immediate transition from colorless to an end point that ranged from dark red to bright orange depending on the pH. These ferric-siderophores (BIS, ferric-bisucaberin; PUT, ferric-putrebactin; AVA, ferric-avaroferrin) native to *Shewanella* and commercially acquired ferric-ferrioxamine E (FER) presented a similar UV-visible spectrum with maximum absorption at ~430 nm, in agreement with the literature (30).

Cyclic voltammograms of the three ferric-siderophores from *Shewanella* (Fig. S5) are complex and dominated by a pair of reduction and oxidation peaks. These peaks portray the speciation found in tetradentate siderophores, where two species are more prevalent in solution for each ferric-siderophore at neutral pH, one with lower reduction potential, and another with a higher reduction potential (Table 2) (31, 32). Of the measured reduction potentials, the species with positive potential can be spontaneously reduced by SfSIP, whereas the reduction of the species with negative potential is thermodynamically an uphill process.

SfSIP reduces hydroxamate siderophores produced by Shewanella

Having shown that SfSIP has adequate thermodynamic properties to reduce ferric-siderophores, its capability to perform the reaction was tested by stopped-flow kinetic assays. SfSIP in the semiquinone state ($SfSIP_{semi}$) was prepared using sodium dithionite (Fig. S6). Upon mixing of $SfSIP_{semi}$ with ferric-siderophores (AVA, BIS, and PUT) absorption spectra changes showed an increase at 470 nm and a decrease at 600 nm (Fig. 2*A*). This is consistent with the transfer of one electron from the semiquinone flavin to the ferric-siderophore yielding fully oxidized SfSIP and Fe^{2+}. Ferric-siderophore reduction was observed for all ferric-siderophores except for FER (Fig. 2*B*). The rate constant of ferric-siderophore reduction was determined (Table 3) from the kinetic trace at 600 nm to avoid signal interference from the ferric-siderophores. All kinetic traces were monophasic except for PUT, which was best fit by a biphasic exponential. This might be a consequence of the presence of small amounts of the other two siderophores (AVA and BIS) in this sample, adding extra minor features to the kinetic trace. All siderophores presented rate constants of similar magnitude in agreement with their reduction potentials (Tables 2 and 3).

Exploring the electron donors of SfSIP

Once the function of SfSIP was confirmed as a ferric-siderophore reductase, the interaction of SfSIP with the putative electron donors was tested.

The interaction of SfSIP with NAD(P)H was explored via ^{31}P NMR spectroscopy. In solution, the two pyrophosphate phosphorus atoms of NADH and NADPH have identical chemical environments giving rise to only one resonance at −11.25 ppm in the ^{31}P NMR spectra. Upon addition of increasing amounts of SfSIP to a solution of either NADH or NADPH, a pattern change was observed in the ^{31}P NMR spectrum where the chemical shifts of the two pyrophosphate phosphorus atoms split from a singlet (−11.25 ppm) to two doublets centered at −11.33 and −11.65 ppm indicating that the local environment of the two phosphate groups becomes different upon interaction with the protein (Fig. 3). Furthermore, given that signals for the free and bound states coexist in the spectra, binding occurs in the slow-exchange regime. Using the relative peak intensities, the concentrations of free and bound species were calculated, allowing the determination of the dissociation constant. NADH and NADPH presented a K_D of 20 ± 5 and 21 ± 6 μM, respectively. K_D values in the micromolar range imply a relatively weak binding, characteristic of electron transfer reactions (33).

NADPH presented an extra resonance at 3.47 ppm, which corresponds to the 2′ phosphorous atom. This signal is unperturbed by binding, indicating that the chemical environment of the 2′ phosphorous atom in the bound form remains similar to what is found in the free form. This result strongly suggests that binding of NADPH to SfSIP occurs through the nicotinamide side of the molecule.

Despite the clear evidence for the interaction of NAD(P)H with SfSIP, no direct reduction of the enzyme by these compounds was observed, nor consumption of NAD(P)H (Fig. S7). This excludes the possibility of a ping-pong mechanism in SfSIP, in contrast to what was proposed for the YqjH protein in *E. coli* and the FscN protein from *T. fusca* (16, 17). In this context, other biologically relevant electron donors for SfSIP were considered. It is reported in the literature that ferric-reductases of the FSR family such as FchR from *Bacillus halodurans* can utilize other electron donors such as ferredoxin (34). The genome of *S. frigidimarina* codes for several small ferredoxins. A ferredoxin from *Clostridium tetanomorphum*, which presents a high sequence identity (39%) with a 4Fe-4S ferredoxin encoded in the genome of *S. frigidimarina* (sequence ID:WP_059746450.1) was used to explore the hypothesis of ferredoxin serving as electron donor for SfSIP.

The reduction of SfSIP by ferredoxin revealed a two-step process characterized by an initial fast decrease in absorbance at 470 nm followed by a slower decrease (Fig. 4). Concomitantly, spectral changes at 600 nm revealed a fast increase in absorbance followed by a slow decrease. Altogether, these changes represent the formation of the semiquinone state followed by the transition to the fully reduced state of the flavin ($FADH_2$). The fact that SfSIP can be fully reduced by ferredoxin shows that it is not restricted to be reduced to a FAD-semiquinone intermediate as proposed for the reduction of IruO from *S. aureus* by NADPH (21).

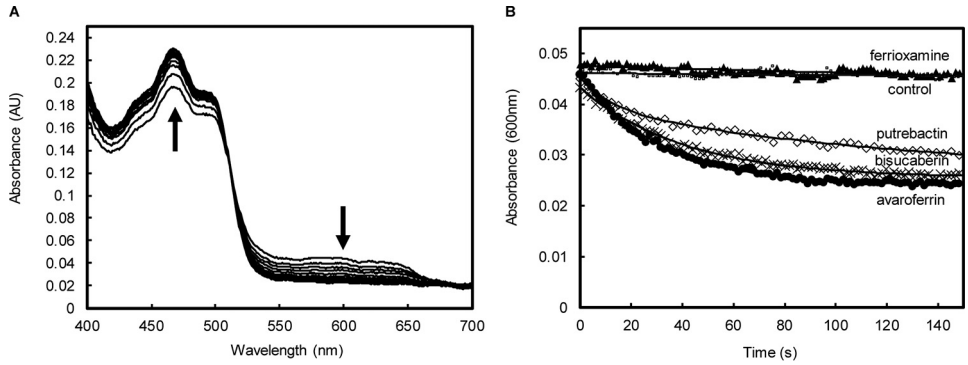

Figure 2. SfSIP-mediated reduction of ferric-siderophores. *A,* absorption spectra changes during 150 s after mixing $SfSIP_{semi}$ with ferric-siderophore avaroferrin. The *up arrow* indicates the increase in absorbance at 470 nm and the *down arrow* indicates a decrease in the absorbance at 600 nm. *B,* time-resolved traces of SfSIP-mediated reduction of ferric-siderophores (600 nm): ▲, ferrioxamine E; ●, avaroferrin; ◇, putrebactin; ×, bisucaberin; □, control (apo-avaroferrin) and the respective fittings (*solid lines*).

Table 3
Rate constants of ferric-siderophore reduction by SfSIP in the semiquinone state

Siderophore	Rate constant (K_{obs})
Avaroferrin	$0.033 \pm 0.001\ s^{-1}$
Bisucaberin	$0.025 \pm 0.001\ s^{-1}$
Ferrioxamine E	
Putrebactin	0.08 ± 0.001 and $0.007 \pm 0.005\ s^{-1}$

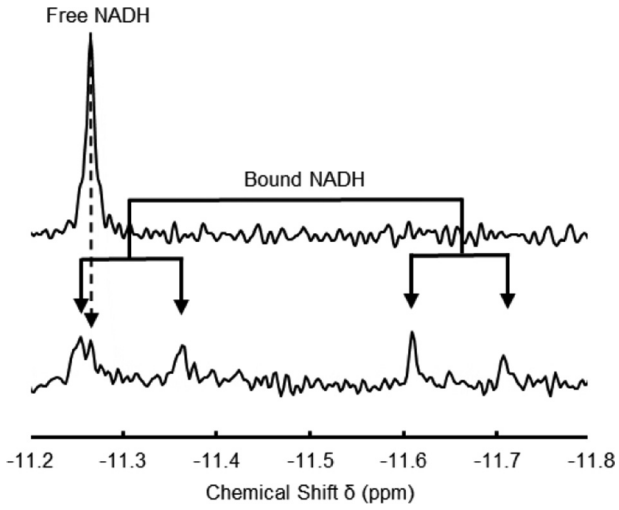

Figure 3. Proton-decoupled ^{31}P NMR spectra. *Top spectrum* corresponds to 100 μM NADH and *bottom spectrum* corresponds to a NADH/SfSIP ratio of 0.58.

Measuring SfSIP-mediated ferrous iron production

To assess the production of ferrous iron by SfSIP using different electron donors and different ferric-siderophores, ferric reductase assays were performed in the presence of the ferrous iron chelator ferrozine. Absorption spectra changes show a gradual increase in absorbance at 562 nm indicating the production of ferrous-ferrozine (Fig. 5). In the absence of SfSIP, no production of ferrous iron was observed (Fig. 5*A*). Ferredoxin and dithionite were able to drive the reduction of ferric-siderophores via SfSIP with ferredoxin presenting the fastest rates for the formation of ferrous iron. Surprisingly, the presence of ferrozine enabled NADH and NADPH to also drive the ferric reductase activity of SfSIP. Furthermore, NADH and NADPH show similar rates of ferrous iron production in agreement with their similar binding constants. The ferrous iron production activity of SfSIP using ferric-avaroferrin was compared for the different electron donors. Using ferredoxin as electron donor the value obtained (55 nmol of Fe^{2+} min^{-} 1 mg^{-1}) compares well with the reduction of fuscachelin by FscN of *T. fusca* using NADH (40 nmol of Fe^{2+} min^{-1} mg^{-1}). By contrast, the values of the ferrous iron production activity of SfSIP using sodium dithionite, NADH, and NADPH (18, 15, and 14 nmol of Fe^{2+} min^{-1} mg^{-1}, respectively) are more similar to the values reported for the ferrous iron production activity of YqhJ using NADPH (22 nmol of Fe^{2+} min^{-1} mg^{-1}).

Additionally, in the presence of ferrozine, SfSIP could reduce all ferric-siderophores tested, including ferrioxamine E, which has a more negative reduction potential (Fig. 5*B*). The formation of ferrous iron was biphasic for all ferric-siderophores except ferrioxamine E, which is monophasic. These data tie with the voltammetric results, suggesting the existence of two iron-coordinated species in solution (Table 2), and reveal that the presence of a Fe^{2+}-scavenger enables SfSIP to reduce iron forms that would otherwise be inaccessible.

Discussion

The characterization of SfSIP revealed several novelties relative to what was previously reported in the literature regarding this class of enzymes. First, it revealed that the length of the C terminus *per se* is not a good proxy for deducing the electron donor of a SIP. Indeed, although sequence comparison and structural analysis placed SfSIP in the SIP family subgroup I that uses NADH, this is the first reported case of a FAD-containing SIP where discrimination between these two electron donors does not occur. The structure of this enzyme suggests that the unprecedented placement of Lys-257 away from the entrance of the NAD(P)H-binding pocket may be responsible for this behavior. No other site in the structure of SfSIP provides access to the FAD cofactor and the placement of Lys-257 makes the triad basic amino acid residue pocket larger compared with the other SIPs from the same subgroup. Second, the observation that SfSIP can use ferredoxin as electron donor is also a first for the SIP family of enzymes. These observations provided two new insights on the reactivity of SIPs. On one hand, the electron donor repertoire of SfSIP is larger than previously reported for other flavin containing SIPs. On the other hand, ferredoxin can directly reduce SfSIP in marked contrast

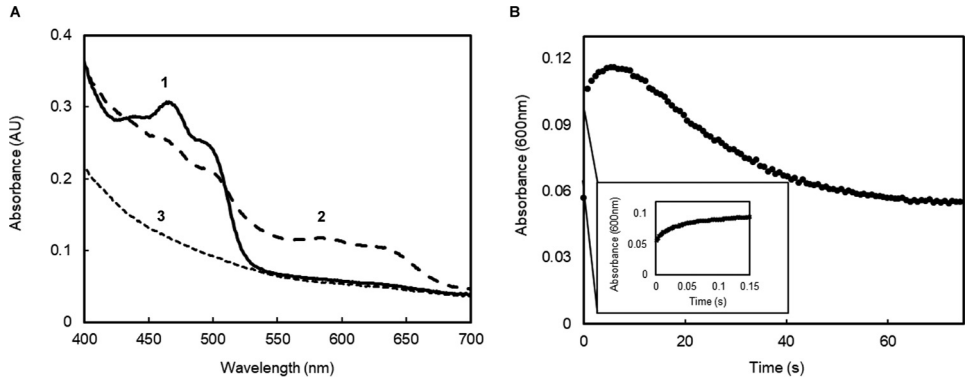

Figure 4. Reduction of SfSIP using a ferredoxin. *A,* absorption spectral changes after mixing ferredoxin with SfSIP. *Numbers* in the figure indicate significant spectral features: *1*) initial spectrum showing the typical features of oxidized SfSIP; *2*) spectrum after 2 s, showing the typical features of the formation of the semi-quinone state of SfSIP; *3*) final spectrum at 75 s, representing fully reduced SfSIP. *B,* time-resolved kinetic trace of SfSIP reduction followed at 600 nm.

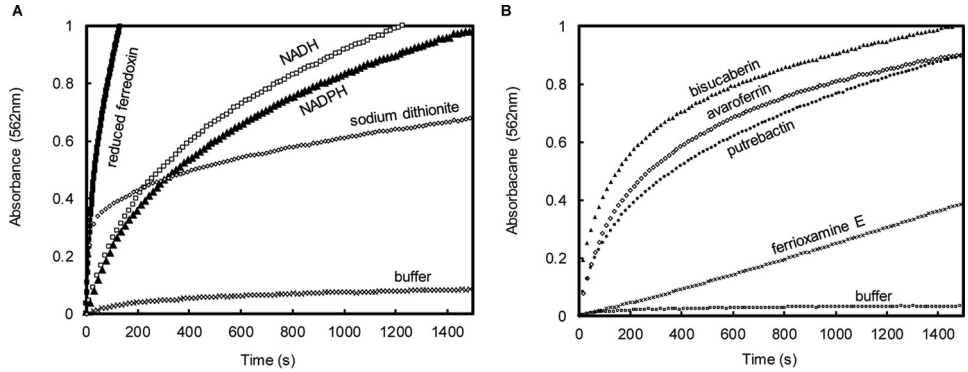

Figure 5. Time-resolved formation of the Fe(II)-ferrozine complex by SfSIP. *A,* experiments performed using ferric-avaroferrin as iron-source and different electron donors. *B,* experiments performed using NADPH as electron donor with different ferric siderophore.

with NAD(P)H, which require the presence of an Fe^{2+}-scavenger. Ferredoxins have two major differences with respect to NAD(P)H, both of which could contribute to different reactivity. Ferredoxins have more negative reduction potentials, and thus a stronger driving force (35). Furthermore, NAD(P)H operate as obligatory two-electron donors, unlike ferredoxins where the 4Fe-4S clusters operate as single electron donors.

Interestingly, the presence of ferrozine in the reaction mixture is sufficient to enable NAD(P)H to function as electron donors. This observation is reminiscent of the redox facilitated ligand exchange mechanism proposed for the reductive release of Fe^{2+} from low potential siderophores in the presence of a seemingly overwhelming unfavorable driving force (14). Ferrozine is known to have a "pulling" effect on reactions involving the formation of Fe^{2+} and caveats for the interpretation of results have been widely disseminated in the literature (36). Nonetheless, in the context of the data reported here, the presence of ferrozine may have provided a glimpse on the role and regulation of SfSIP in the context of iron uptake by *Shewanella*. Although ferrozine is not a physiologically relevant ligand, it provides an *in vitro* mimetic of naturally occurring ferrous iron ligands such as porphyrins or apo-proteins that promote concurrent ferric-siderophore reduction and ferrous iron uptake (36, 37). *Shewanella* are notorious for maintaining a high level of intracellular iron content but the process is by no means unregulated. This situation would be extraordinarily dangerous for these organisms that are found in environmental niches in oxic–anoxic transition zones, due to the participation of Fe^{2+} in the production of reactive species through the Haber–Weiss cycle (14). Proteins of the siderophore pathway such as the archetypal SIP, ViuB, are typically under the control of the Fur regulon (22). However, in *S. frigidimarina*, the Arc (aerobic respiration control) signal transduction system appears to be the best candidate for this role, given the fact that the SfSIP gene is found downstream of a putative ArcA-binding sequence (38, 39). This genetic context together with the functional characterization of SfSIP allow us to formulate a hypothesis for the overall regulation of its activity *in vivo*. Expression of SfSIP is likely controlled by the Arc transcriptional regulator, based on environmental cues indicating changes of oxygen availability. When oxygen levels are extremely low, cellular iron demand is increased and expression of SfSIP is up-regulated contributing to iron uptake without competing for its use because it is a flavoprotein. Furthermore, when cells find themselves in a reducing environment where synthesis of numerous iron containing proteins is stimulated in *Shewanella,* the pool of reduced ferredoxins is increased because of the favorable redox environment (39, 40). Reduced ferredoxins donate electrons to SfSIP, boosting the availability of intracellular iron given that they do not require the presence of Fe^{2+}-acceptors and enable SfSIP to reduce ferric siderophore species of lower reduction potential. In contrast, when oxygen levels increase, the redox conditions are less favorable to the main-

tenance of a pool of reduced ferredoxins and the risk of producing reactive species is higher. Therefore, NAD(P)H can drive the reduction of ferric-siderophores only when a downstream acceptor is ready to receive the ferrous iron. This ensures that metabolic reducing power is only diverted to this activity when it is required without compromising cell integrity.

In conclusion, the novel aspects of SfSIP's reactivity revealed in this work offer opportunities to interfere with the iron metabolism of *Shewanella* at the level of SfSIP and its homologues. However, further knowledge is necessary to understand if the function and regulation of SIPs is conserved among the different species of *Shewanella. Shewanella* are notorious for having multiple redundant metabolic pathways that may hinder the identification of a clear-cut phenotype for SfSIP and its homologues (41, 42). However, studies using animal models have shown that knock-out of SIP genes greatly diminishes the virulence of pathogenic bacteria, revealing the importance of these proteins for survival fitness (43). This makes ferric reductases such as SfSIP, *bona fide* targets to disturb iron homeostasis in a wide diversity of microbial pathogens, contributing in this way, to avert losses derived from food spoilage and infections caused by *Shewanella* (44).

Experimental procedures

Expression and purification of SfSIP

SFRI_RS12295 gene from *S. frigidimarina NCIM400* was inserted into pETBlue-1 expression vector (Novagen). Transformed *E. coli* Tuner (DE3) pLacI cells were grown for the overexpression of SIP in Luria-Bertani (LB) medium, supplemented with autoinduction solutions and selective antibiotics as previously described (23). Cells were grown at 30 °C for 32 h before collection, and the supernatant was purified by ion exchange chromatography as previously reported (23). The purity of SfSIP was assessed using SDS-PAGE analysis and UV-visible spectroscopy, and the SfSIP's sequence was confirmed via N-terminal sequencing.

Structure determination of SfSIP

SfSIP was crystallized using 22% PEG 3350 and 0.22 M magnesium formate dihydrate as precipitant by the hanging drop vapor diffusion method, where 1 μl of precipitant was mixed with 1 μl of a 30 mg/ml of protein solution and equilibrated against a 500-μl reservoir. Crystals were harvested and flash-cooled in liquid nitrogen directly from the crystallization drop, and diffraction data were collected at 100 K to a resolution of 1.35 Å on Diamond Light Source (DLS) beamline I04 (Didcot, UK) (23). The images were processed with xia2 (45), which makes use of XDS (46) and the CCP4 suite (47) for integration and conversion of integrated intensities to structure factors. The structure was solved by molecular replacement using PHASER in the CCP4 suite (47) and a previously determined SIP crystal structure (PDB 4YHB) (17) as phasing model to a resolution of 1.4 Å. The model was corrected and completed with COOT (48) after an initial refinement using REFMAC5 in the CCP4 suite (49). However, the subsequent refinement led to unsatisfactory values of *R* and *R*-free of 22.3 and 22.9%, respectively, and it was decided to use data collected from another crystal for structure determination and refinement.

Table 4
Data collection and refinement statistics

	Native
Beamline and detector	DLS I04, PILATUS 6 M
Space group	$P\,2_1$
Unit cell parameters (Å, °)	$a = 38.10$, $b = 77.75$, $c = 44.92$, $\beta = 109.64$
Resolution (Å)	28.62–1.15 (1.19–1.15)
Unique reflections	86,403 (8,002)
Completeness (%)	99.0 (91.6)
Multiplicity	5.0 (3.6)
R_{merge} (%)[a]	3.63 (44.6)
R_{meas} (%)[b]	4.05 (48.6)
CC1/2	1 (0.795)
$\langle I/\sigma(I)\rangle$	18.4 (2.4)
Wilson plot B (Å^2)	12.0
Refinement	
Resolution limits (Å)	28.62–1.15 (1.19–1.15)
R-factor (%)[c]	14.5 (24.7)
No. reflections	86396
Free *R*-factor (%)[d]	17.4 (27.6)
Model composition	
Non-hydrogen protein atoms	2,274
Solvent molecules	431
FAD ligand	105
Model r.m.s. deviations from ideality	
Bond lengths (Å)	0.009
Bond angles (°)	1.38
Model completeness and validation	
Regions omitted	1–8 and 20–23
Mean B values (Å^2)[e]	
Protein	16.9
Solvent molecules	30.2
FAD ligand	18.6
Ramachandran plot	
Most favored regions (%)	100.0

[a] R_{merge} = merging *R*-factor, $(\Sigma_{hkl}\Sigma_i|I_i(hkl) - \langle I(hkl)\rangle|)/(\Sigma_{hkl}\Sigma_i I(hkl)) \times 100\%$.
[b] R_{meas} = redundancy independent *R*-factor, $\Sigma_h[N_{hkl}/(N_{hkl}-1)]^{1/2}\Sigma_i|I_i(hkl) - \langle I(hkl)\rangle|/\Sigma_{hkl}\Sigma_i I_i(hkl) \times 100\%$, where *I* is the observed intensity, $\langle I\rangle$ is the average intensity of multiple observations from symmetry-related reflections, and N_{hkl} is their multiplicity (58).
[c] *R*-factor $= \Sigma_{hkl}||F_o|-|F_c||/\Sigma_{hkl}|F_o|$, where $|F_o|$ and $|F_c|$ are the observed and calculated structure factor amplitudes, respectively.
[d] Free *R*-factor is the cross-validation *R*-factor computed from a randomly chosen subset of 5% of the total number of reflections, which were not used during the refinement.
[e] Calculated from the equivalent isotropic *B* values.

The second crystal was obtained under the same crystallization conditions as the first, with the difference that 1 mM ferric-siderophore (bisucaberin), dissolved in DMSO, was added to the protein solution prior to setting up the crystallization experiment, and it was soaked for 1 min in a mother liquor solution to which 200 μM NADPH (dissolved in 20 mM Tris-HCl, pH 7.6, 150 mM NaCl) was added prior to flash cooling in liquid nitrogen. Diffraction data at 100 K were collected to 1.15 Å resolution on DLS beamline I04 and the images were likewise processed with xia2. The data collection and processing statistics are listed in Table 4. The structure was solved using molecular replacement and the previously determined structure of SfSIP as a template. Structure refinement was performed using PHENIX (50). Throughout the refinement, the model was periodically checked and corrected with COOT against $2|F_o| - |F_c|$ and $|F_o| - |F_c|$ electron-density maps. Solvent molecules were added automatically by PHENIX and validated by inspection of electron-density maps in COOT (48). In the final refinement cycles, hydrogen atoms were included in calculated positions with the PHENIX READYSET tool and anisotropic displace-

ment parameters were refined for nonhydrogen protein atoms. The final values of *R* and *R*-free (51) were 14.5 and 17.4%, respectively, and the maximum likelihood estimate of the overall coordinate error was 0.1 Å. The model stereochemical quality was analyzed with MOLPROBITY (52) and there are no outliers in the Ramachandran (54) ψ,ϕ plot. The final refinement statistics are included in Table 4. The coordinates and structure factors have been submitted to the Protein Data Bank in Europe (53) with accession codes 6GEH and r6GEHsf. Pictures were produced using PyMOL.

PFV experiments

Experiments were performed on a pyrolytic graphite edge (PGE) electrode purchased from IJ Cambria Scientific at 25 °C using a three-electrode electrochemical cell configuration with the PGE (working electrode), a platinum wire (counter electrode), and an Ag/AgCl (3 M KCl) (reference electrode) inside a Coy anaerobic chamber using an electrochemical analyzer from CHI Instruments controlled by the manufacturer's software (version 10.12). Oxygen levels were kept stable at ~8 ppm. The electrode was cleaned (3 M nitric acid and distilled water) and freshly polished before every experiment. SfSIP was immobilized in the freshly polished PGE electrode by pipetting 3 μl of SIP in 20 mM potassium phosphate buffer, 100 mM KCl, pH 7.6. To guarantee protein immobilization, the electrode was left to dry for ~15 min. Excess and/or unattached protein was removed by rinsing the electrode with distilled water. The electrode was then immersed in 2 ml of a mixed buffer solution containing 5 mM HEPES, 5 mM CHES, and 5 mM MES at the following pH values: 5.5, 6, 7.8, and 8.5. For each pH, voltammograms were acquired at the following scan rates (mV s^{-1}): 10, 13, 17, 21, 28, 36, 41, 48, 60, 78, 100, 130, 170, 210, 280, 360, 410, 480, 600, 780, 1,000, 1,300, 1,700, 2,100, 2,800, 3,600, 4,100, 4,800, 6,000, 7800, 9,100, and 10,000 to ensure uniform data point coverage in a logarithmic scale plot. After each experiment, the solution was removed, and the pH was measured. These experiments were performed in duplicate by cleaning the electrode and repeating the procedure. Using the program Qsoas, the background current was subtracted for every voltammogram and all data were analyzed with Excel. The trumpet plots were fitted using the Butler-Volmer model using Jellyfit with the following parameters: $n = 1$, potential step 1×10^{-6}, and temperature 25 °C; for every data potential a standard deviation (S.D.) of 0.005 was assumed (25, 27). Potentials were reported in mV *versus* the SHE by addition of 210 mV to those measured (54).

Production of ferric-siderophores

A deep-sea sediment metagenomic library was constructed and the *mbs* gene cluster (*mbsA-D*) was cloned as previously reported (29). As it tested positive for siderophore activity with the chrome azurol S assay, the metagenome-derived *mbs* cluster clone was cultured for 3 days at 37 °C in LB medium supplemented with isopropyl 1-thio-β-D-galactopyranoside (100 μM) and chloramphenicol (30 μg/ml). Centrifuge-clarified supernatant was extracted using a C18 resin, then eluted with a stepwise aqueous-MeOH gradient system. Fractions containing siderophores were further purified by Sephadex LH-20 gel filtration. Chrome azurol S active fractions were combined and further purified by two steps of a C18 HPLC using aqueous-MeOH (containing 0.2% acetic acid) gradient system to afford purified bisucaberin, putrebactin, and avaroferrin (29). The purity and nature of siderophore-containing samples was assessed by LC-MS analysis and NMR spectroscopy.

Characterization of ferric siderophores avaroferrin, bisucaberin, putrebactin, and ferrioxamine E

FER (1,12,23-Trihydroxy-1,6,12,17,17,23,28-hexaazacyclotritriacontane-2,5, 13,16,24,27-hexone iron(III) complex) was purchased from Sigma. A 2 mM stock solution was prepared in 20 mM potassium phosphate, 100 mM KCl buffer, pH 7.6.

The apo-siderophores (AVA, BIS, and PUT) were dissolved in DMSO and iron-containing siderophores were prepared for every experiment in working stocks of 500 μM in 20 mM phosphate buffer, 100 mM KCl, pH 7.6. Each 500 μM ferric-siderophore solution was prepared from the starting stock plus equivalent amounts of $FeCl_3$, resulting in an iron-siderophore molar ratio of 1:1.

Cyclic voltammetry experiments were performed at 25 °C using a three-electrode electrochemical cell configuration with the PGE (working electrode), a platinum wire (counter electrode), and an Ag/AgCl (3 M KCl) (reference electrode) inside a Coy anaerobic chamber using an electrochemical analyzer from CHI Instruments controlled by the manufacturer's software (version 10.12). Oxygen levels were kept stable at ~8 ppm. In each experiment, the freshly polished PGE electrode was first immersed in buffer to draw a baseline of the capacitive current and then immersed in the 500 μM ferric-siderophore–containing solution. Scans were acquired at 100 mV s^{-1} in triplicate. All data were analyzed using Excel and QSoas (25). Potentials were determined using the average of the oxidation and reduction peaks and reported in millivolts and with respect to the SHE by addition of 210 mV to those measured (54).

NMR interaction studies

NAD(P)H and SfSIP were prepared in 20 mM Tris-HCl, 100 mM KCl, pH 8, containing 10% D_2O (99.9 atom %). Samples of 100 μM NAD(P)H were titrated against increasing concentrations of SfSIP. To determine the concentration of free and bound species triplicate experiments using a molar ratio of 0.58 (NAD(P)H:SIP) were performed. Using the standard Bruker pulse program "zgdc," one-dimensional proton-decoupled ^{31}P spectra were acquired with 1024 scans, $d1$ of 1.3 s at 25 °C on a Bruker Avance II 500 MHz equipped with a SEX probe for ^{31}P detection.

Collected spectra were visualized and analyzed using TopSpin 3.5 (Bruker). The concentration of free and bound species was determined from the relative intensity of each peak and the dissociation constant (K_D) was calculated using the following equation.

$$K_D = \frac{K_{off}}{K_{on}} = \frac{[A][B]}{[A,B]} \quad \text{(Eq. 1)}$$

Kinetic studies

The kinetic experiments were performed in HI-TECH Scientific Stopped-flow equipment (SF-61DX2) installed inside an anaerobic glove box (Mbraun MB150-GI). The temperature of the drive syringes and mixing chamber was maintained at 25 °C using a water bath, and the pH controlled with 20 mM potassium phosphate buffer, 100 mM KCl, pH 7.6. The time course of the reactions was monitored using a photodiode array. Solutions were prepared inside the anaerobic chamber with degassed water and all experiments were performed in triplicate. Data were analyzed using Excel and fits were performed and analyzed using Kinetics Studio version 2.32 (TgK Scientific).

Reduction of SfSIP with NAD(P)H, sodium dithionite, and ferredoxin

Experiments were performed at multiple time scales and at different concentrations for each reducing agent. The reduction of SfSIP with NAD(P)H was attempted using 0.5 mM NAD(P)H and also using a large excess of NAD(P)H with 10 μM SIP with spectra acquisition for a total 4000 s (67 min).

Reduction of SfSIP with sodium dithionite was performed using 50 μM sodium dithionite with 10 μM SIP. Reduction rates were obtained from experiments at the 6000-s time scale with a total of 200 spectra acquired.

The purity of the ferredoxin from *C. tetanomorphum* was confirmed by SDS-PAGE (15%). To avoid direct reduction of SIP with sodium dithionite the reduction of ferredoxin was carried out in a 1:1 molar ratio and the mixture was left to react for 10 min before initializing the experiments of reduced ferredoxin against SIP. The stock solutions of sodium dithionite were quantified by measuring the absorbance at 315 nm using the molar extinction coefficient of 8043 M^{-1} cm^{-1} (55). Reduction of 10 μM SfSIP was performed using 10 μM reduced ferredoxin.

Reduction of ferric siderophores

Reduction of ferric siderophores (AVA, BIS, PUT, and FER) by reduced SfSIP was performed after reducing SfSIP with sodium dithionite in a 1:1 molar ratio. The reduction of ferric-siderophores was performed using 10 μM SfSIP with 50 μM ferric-siderophores in the stopped-flow apparatus. The reduction rate constants were obtained from fitting the kinetic traces at 600 nm in a 150-s time scale (Table S1).

The ferrozine assay

The ferrozine assay monitored the formation of ferrous iron using an iron chelator with high affinity for Fe^{2+} and ferrozine, purchased from Fluka. The assay was performed with the following components: the Fe^{2+} chelator (0.25 mM ferrozine), the putative siderophore reductase (5 μM SIP), a reducing agent (0.25 mM NAD(P)H, 25 μM sodium dithionite, or 5 μM reduced ferredoxin), and 50 μM for each ferric-siderophore (AVA, BIS, PUT, and FER). The formation of Fe^{2+}-ferrozine complexes was analyzed by measuring the absorbance at 562 nm (56, 57). Each experiment was performed in triplicate and controls were performed containing all the previously described components except for SIP.

Author contributions—I. B. T., J. M. S., B. M. F., T. C., P. M. M., E. M., and R. O. L. formal analysis; I. B. T., J. M. S., B. M. F., T. C., P. M. M., E. M., and R. O. L. investigation; I. B. T., P. M. M., E. M., and R. O. L. writing-original draft; I. B. T. and R. O. L. writing-review and editing; M. F. resources; R. O. L. conceptualization; R. O. L. supervision.

Acknowledgments—We thank Isabel Pacheco for help in the purification of SfSIP and Dr. Américo Duarte for providing ferredoxin. We also thank all members of the Inorganic Biochemistry and NMR Laboratory for discussions and comments and feedback regarding the preparation of the manuscript. The NMR experiments were performed at CERMAX (Centro de Ressonância Magnetica António Xavier) and was financially supported by Project LISBOA-01-0145-FEDER-007660 (Microbiologia Molecular, Estrutural e Celular) funded by FEDER funds through COMPETE2020-Programa Operacional Competitividade e Internacionalização (POCI), the European Community's Seventh Framework Program (FP7/2007–2013)) under Grant Agreement 283570 (BioStruct-X). Beamtime at I04 at the Diamond Light Source and assistance from the beamline staff during the synchrotron data collections are gratefully acknowledged.

References

1. Janda, J. M., and Abbott, S. L. (2014) The genus *Shewanella*: from the briny depths below to human pathogen. *Crit. Rev. Microbiol.* **40,** 293–312 Medline
2. Janda, J. M. (2014) *Shewanella*: a marine pathogen as an emerging cause of human disease. *Clin. Microbiol. Newsl.* **36,** 25–29 CrossRef
3. Ghosal, D., Omelchenko, M. V., Gaidamakova, E. K., Matrosova, V. Y., Vasilenko, A., Venkateswaran, A., Zhai, M., Kostandarithes, H. M., Brim, H., Makarova, K. S., Wackett, L. P., Fredrickson, J. K., and Daly, M. J. (2005) How radiation kills cells: survival of *Deinococcus radiodurans* and *Shewanella oneidensis* under oxidative stress. *FEMS Microbiol. Rev.* **29,** 361–375 CrossRef Medline
4. Bowman, J. P., McCammon, S. A., Nichols, D. S., Skerratt, J. H., Rea, S. M., Nichols, P. D., and McMeekin, T. A. (1997) *Shewanella gelidimarina* sp. nov., and *Shewanella frigidimarina* sp. nov., novel Antarctic species with the ability to produce eicosapentaenoic acid (20:5 ω3) and grow anaerobically by dissimilatory Fe(III) reduction. *Int. J. Syst. Bacteriol.* **47,** 1040–1047 CrossRef Medline
5. Linares, D., Jean, N., Van Overtvelt, P., Ouidir, T., Hardouin, J., Blache, Y., and Molmeret, M. (2016) The marine bacteria *Shewanella frigidimarina* NCIMB400 upregulates the type VI secretion system during early biofilm formation. *Environ. Microbiol. Rep.* **8,** 110–121 CrossRef Medline
6. Martin, J. H., and Michael Gordon, R. (1988) Northeast Pacific iron distributions in relation to phytoplankton productivity. *Deep Sea Res. Part A Oceanogr. Res. Pap.* **35,** 177–196 CrossRef
7. Fonseca, B. M., Paquete, C. M., Salgueiro, C. A., and Louro, R. O. (2012) The role of intramolecular interactions in the functional control of multiheme cytochromes *c*. *FEBS Lett.* **586,** 504–509 CrossRef Medline
8. Martin, J. H. (1990) Glacial-interglacial CO_2 change: the iron hypothesis. *Paleocenography* **5,** 1–13 CrossRef
9. Moore, J. K., and Doney, S. C. (2007) Iron availability limits the ocean nitrogen inventory stabilizing feedbacks between marine denitrification and nitrogen fixation. *Global Biogeochem. Cycles* **21,** 1–12
10. Moore, C. M., Mills, M. M., Arrigo, K. R., Berman-Frank, I., Bopp, L., Boyd, P. W., Galbraith, E. D., Geider, R. J., Guieu, C., Jaccard, S. L., Jickells, T. D., La Roche, J., Lenton, T. M., Mahowald, N. M., Marañón, E., *et al.* (2013) Processes and patterns of oceanic nutrient limitation. *Nat. Geosci.* **6,** 701–710 CrossRef
11. Yang, Y., Harris, D. P., Luo, F., Xiong, W., Joachimiak, M., Wu, L., Dehal, P., Jacobsen, J., Yang, Z., Palumbo, A. V., Arkin, A. P., and Zhou, J. (2009) Snapshot of iron response in *Shewanella oneidensis* by gene network reconstruction. *BMC Genomics* **10,** 131 CrossRef Medline

12. Koebnik, R. (2005) TonB-dependent trans-envelope signalling: the exception or the rule? *Trends Microbiol.* **13,** 343–347 CrossRef Medline
13. Miethke, M., and Marahiel, M. A. (2007) Siderophore-based iron acquisition and pathogen control. *Microbiol. Mol. Biol. Rev.* **71,** 413–451 CrossRef Medline
14. Boukhalfa, H., and Crumbliss, A. L. (2002) Chemical aspects of siderophore mediated iron transport. *BioMetals* **15,** 325–339 CrossRef Medline
15. Holden, V. I., and Bachman, M. A. (2015) Diverging roles of bacterial siderophores during infection. *Metallomics* **7,** 986–995 CrossRef Medline
16. Miethke, M., Hou, J., and Marahiel, M. A. (2011) The siderophore-interacting protein YqjH acts as a ferric reductase in different iron assimilation pathways of *Escherichia coli*. *Biochemistry* **50,** 10951–10964 CrossRef Medline
17. Li, K., Chen, W. H., and Bruner, S. D. (2015) Structure and mechanism of the siderophore-interacting protein from the fuscachelin gene cluster of *Thermobifida fusca*. *Biochemistry* **54,** 3989–4000 CrossRef Medline
18. Sedlácek, V., van Spanning, R. J., and Kučcra, I. (2009) Ferric reductase A is essential for effective iron acquisition in *Paracoccus denitrificans*. *Microbiology* **155,** 1294–1301 CrossRef Medline
19. Fontecave, M., Covès, J., and Pierre, J. L. (1994) Ferric reductases or flavin reductases? *Biometals* **7,** 3–8 Medline
20. Coves, J., and Fontecave, M. (1993) Reduction and mobilization of iron by a NAD(P)H: flavin oxidoreductase from *Escherichia coli*. *Eur. J. Biochem.* **211,** 635–641 CrossRef Medline
21. Kobylarz, M. J., Heieis, G. A., Loutet, S. A., and Murphy, M. E. P. (2017) Iron uptake oxidoreductase (IruO) uses a flavin adenine dinucleotide semiquinone intermediate for iron-siderophore reduction. *ACS Chem. Biol.* **12,** 1778–1786 CrossRef Medline
22. Butterton, J. R., and Calderwood, S. B. (1994) Identification, cloning, and sequencing of a gene required for ferric vibriobactin utilization by *Vibrio cholerae*. *J. Bacteriol.* **176,** 5631–5638 CrossRef Medline
23. Trindade, I. B., Fonseca, B. M., Matias, P. M., Louro, R. O., and Moe, E. (2016) A putative siderophore-interacting protein from the marine bacterium *Shewanella frigidimarina* NCIMB 400: cloning, expression, purification, crystallization and X-ray diffraction analysis. *Acta Crystallogr. Sect. Struct. Biol. Commun.* **72,** 667–671 CrossRef
24. Wallace, A. C., Laskowski, R. A., and Thornton, J. M. (1995) Ligplot: a program to generate schematic diagrams of protein ligand interactions. *Protein Eng.* **8,** 127–134 CrossRef Medline
25. Fourmond, V. (2016) QSoas: a versatile software for data analysis. *Anal. Chem.* **88,** 5050–5052 CrossRef Medline
26. Louro, R. O., Catarino, T., Salgueiro, C. A., LeGall, J., and Xavier, A. (1996) V Redox-Bohr effect in the tetrahaem cytochrome *c*3 from *Desulfovibrio vulgaris*: a model for energy transduction mechanisms. *J. Biol. Inorg. Chem.* **1,** 34–38 CrossRef
27. Jeuken, L. J. C., McEvoy, J. P., and Armstrong, F. A. (2002) Insights into gated electron-transfer kinetics at the electrode-protein interface: a square wave voltammetry study of the blue copper protein azurin. *J. Phys. Chem. B* **106,** 2304–2313 CrossRef
28. Armstrong, F. A., Heering, H. A., Hirst, J., Armstrong, F. A., Heering, H. A., and Hirst, J. (1997) Reactions of complex metalloproteins studied by protein-film voltammetry. *Chem. Soc. Rev.* **26,** 169–173 Medline
29. Fujita, M. J., and Sakai, R. (2014) Production of avaroferrin and putrebactin by heterologous expression of a deep-sea metagenomic DNA. *Mar. Drugs.* **12,** 4799–4809 CrossRef Medline
30. Rütschlin, S., Gunesch, S., and Böttcher, T. (2017) One enzyme, three metabolites: *Shewanella algae* controls siderophore production via the cellular substrate pool. *Cell Chem. Biol.* **24,** 598–604.e10 CrossRef Medline
31. Hou, Z., Raymond, K. N., O'Sullivan, B., Esker, T. W., and Nishio, T. (1998) A preorganized siderophore: thermodynamic and structural characterization of alcaligin and bisucaberin, microbial macrocyclic dihydroxamate chelating agents. *Inorg. Chem.* **37,** 6630–6637 CrossRef Medline
32. Spasojevic, I., Armstrong, S. K., Brickman, T. J., and Crumbliss, A. L. (1999) Electrochemical behavior of the Fe(III) complexes of the cyclic hydroxamate siderophores alcaligin and desferrioxamine E. *Inorg. Chem.* **38,** 449–454 CrossRef Medline
33. Díaz-quintana, A., Cruz-gallardo, I., Rosa, M. A. De, and Díaz-moreno, I. (2017) Diversity of interactions in redox systems: from short- to long-lived complexes. in *Redox Proteins in Supercomplexes and Signalosomes* (Louro, R. O., and Díaz-moreno, I., eds) pp. 1–48, CRC Press, Boca Raton, FL
34. Miethke, M., Pierik, A. J., Peuckert, F., Seubert, A., and Marahiel, M. A. (2011) Identification and characterization of a novel-type ferric siderophore reductase from a Gram-positive extremophile. *J. Biol. Chem.* **286,** 2245–2260 CrossRef Medline
35. Atkinson, J. T., Campbell, I., Bennett, G. N., and Silberg, J. J. (2016) Cellular assays for ferredoxins: a strategy for understanding electron flow through protein carriers that link metabolic pathways. *Biochemistry* **55,** 7047–7064 CrossRef Medline
36. Pierre, J. L., Fontecave, M., and Crichton, R. R. (2002) Chemistry for an essential biological process. *BioMetals* **15,** 341–346 CrossRef Medline
37. Baysse, C., Matthijs, S., Schobert, M., Layer, G., Jahn, D., and Cornelis, P. (2003) Co-ordination of iron acquisition, iron porphyrin chelation and iron-protoporphyrin export via the cytochrome *c* biogenesis protein CcmC in *Pseudomonas fluorescens*. *Microbiology* **149,** 3543–3552 CrossRef Medline
38. Gralnick, J. A., Brown, C. T., and Newman, D. K. (2005) Anaerobic regulation by an atypical Arc system in *Shewanella oneidensis*. *Mol. Microbiol.* **56,** 1347–1357 CrossRef Medline
39. Gao, H., Wang, X., Yang, Z. K., Palzkill, T., and Zhou, J. (2008) Probing regulon of ArcA in *Shewanella oneidensis* MR-1 by integrated genomic analyses. *BMC Genomics* **9,** 42 CrossRef Medline
40. Beliaev, A. S., Klingeman, D. M., Klappenbach, J. A., Wu, L., Romine, M. F., Tiedje, J. M., Nealson, K. H., Fredrickson, J. K., and Zhou, J. (2005) Global transcriptome analysis of *Shewanella oneidensis* MR-1 exposed to different terminal electron acceptors. *J. Bacteriol.* **187,** 7138–7145 CrossRef Medline
41. Fonseca, B. M., Paquete, C. M., Neto, S. E., Pacheco, I., Soares, C. M., and Louro, R. O. (2013) Mind the gap: cytochrome interactions reveal electron pathways across the periplasm of *Shewanella oneidensis* MR-1. *Biochem. J.* **449,** 101–108 CrossRef Medline
42. Sturm, G., Richter, K., Doetsch, A., Heide, H., Louro, R. O., and Gescher, J. (2015) A dynamic periplasmic electron transfer network enables respiratory flexibility beyond a thermodynamic regulatory regime. *ISME J.* **9,** 1802–1811 CrossRef Medline
43. Tu, J., Lu, F., Miao, S., Ni, X., Jiang, P., Yu, H., Xing, L., Yu, S., Ding, C., and Hu, Q. (2014) The siderophore-interacting protein is involved in iron acquisition and virulence of *Riemerella anatipestifer* strain CH3. *Vet. Microbiol.* **168,** 395–402 CrossRef Medline
44. Xu, N., Qian, K., Dong, Y., Chen, Y., Yu, Q., Zhang, B., Xing, L., and Li, M. (2014) Novel role of the *Candida albicans* ferric reductase gene CFL1 in iron acquisition, oxidative stress tolerance, morphogenesis and virulence. *Res. Microbiol.* **165,** 252–261 CrossRef Medline
45. Winter, G. (2010) xia2: an expert system for macromolecular crystallography data reduction. *J. Appl. Crystallogr.* **43,** 186–190 CrossRef
46. Kabsch, W. (2010) XDS. *Acta Crystallogr D Biol. Crystallogr.* **66,** 125–132 CrossRef Medline
47. Winn, M. D., Ballard, C. C., Cowtan, K. D., Dodson, E. J., Emsley, P., Evans, P. R., Keegan, R. M., Krissinel, E. B., Leslie, A. G., McCoy, A., McNicholas, S. J., Murshudov, G. N., Pannu, N. S., Potterton, E. A., Powell, H. R., *et al.* (2011) Overview of the CCP4 suite and current developments. *Acta Crystallogr. D Biol. Crystallogr.* **67,** 235–242 CrossRef Medline
48. Emsley, P., Lohkamp, B., Scott, W. G., and Cowtan, K. (2010) Features and development of Coot. *Acta Crystallogr. D Biol. Crystallogr.* **66,** 486–501 CrossRef Medline
49. Murshudov, G. N., Vagin, A. A., and Dodson, E. J. (1997) Refinement of macromolecular structures by the maximum-likelihood method. *Acta Crystallogr. D Biol. Crystallogr.* **53,** 240–255 CrossRef Medline
50. Adams, P. D., Afonine, P. V., Bunkóczi, G., Chen, V. B., Davis, I. W., Echols, N., Headd, J. J., Hung, L. W., Kapral, G. J., Grosse-Kunstleve, R. W., McCoy, A. J., Moriarty, N. W., Oeffner, R., Read, R. J., Richardson, D. C., *et al.* (2010) PHENIX: a comprehensive Python-based system for macromolecular structure solution. *Acta Crystallogr. Sect. D Biol. Crystallogr.* **66,** 213–221 CrossRef

51. Brünger, A. T. (1992) Free R value: a novel statistical quantity for assessing the accuracy of crystal structures. *Nature* **355,** 472–475 CrossRef Medline
52. Chen, V. B., Arendall, W. B., 3rd, Headd, J. J., Keedy, D. A., Immormino, R. M., Kapral, G. J., Murray, L. W., Richardson, J. S., and Richardson, D. C. (2010) MolProbity: all-atom structure validation for macromolecular crystallography. *Acta Crystallogr. D Biol. Crystallogr.* **66,** 12–21 CrossRef Medline
53. Velankar, S., Best, C., Beuth, B., *et al.* (2010) PDBe: protein data bank in Europe. *Nucleic Acids Res.* **38,** D308–D317 CrossRef Medline
54. Friis, E. P., Andersen, J. E. T., Madsen, L. L., Bonander, N., Moller, P., and Ulstrup, J. (1998) Dynamics of *Pseudomonas aeruginosa* azurin and its Cys3Ser mutant at single-crystal gold surfaces investigated by cyclic voltammetry and atomic force microscopy. *Electrochim. Acta* **43,** 1114–1122 CrossRef
55. Yousafzai, F. K., and Eady, R. R. (2002) Dithionite reduction kinetics of the dissimilatory copper-containing nitrite reductase of *Alcalegenes xylosoxidans*: the SO_2^- radical binds to the substrate binding type 2 copper site before the type 2 copper is reduced. *J. Biol. Chem.* **277,** 34067–34073 CrossRef Medline
56. Viollier, E., Inglett, P. W., Hunter, K., Roychoudhury, A. N., and Van Cappellen, P. (2000) The ferrozine method revisited: Fe(II)/Fe(III) determination in natural waters. *Appl. Geochem.* **15,** 785–790 CrossRef
57. Jeitner, T. M. (2014) Optimized ferrozine-based assay for dissolved iron. *Anal. Biochem.* **454,** 36–37 CrossRef Medline
58. Diederichs, K., and Karplus, P. A. (1997) Improved R-factors for diffraction data analysis in macromolecular crystallography. *Nat. Struct. Biol.* **4,** 269–275 CrossRef Medline